

# Performance Analysis of IRS-aided Short-Packet NOMA Systems over Nakagami- $m$ Fading Channels

Lei Yuan, *Member, IEEE*, Qiuyu Du, Nan Yang, *Senior Member, IEEE*, Fang Fang, *Member, IEEE*, Nan Yang

**Abstract**—This paper analyzes the performance of an intelligent reflecting surface (IRS)-aided short-packet communication system over Nakagami- $m$  fading channels. In this system, the base station adopts non-orthogonal multiple access (NOMA) to transmit to a near user and a far user, and its transmission to the far user is aided by the IRS. Both continuous phase shifts (CPSs) and discrete phase shifts (DPSs) are considered for the IRS. By using order statistic and moment matching, we approximate the end-to-end channel gain to follow the Gamma distribution and then derive the approximate closed-form expressions for the average block error rate (BLER) in the high signal-to-noise ratio (SNR) regime and then conduct a refined analysis of the interplay among the minimum common blocklength, optimal power allocation, and the related parameters of IRS (e.g., the number of elements of the IRS) for achieving target BLERs at two users. Finally, numerical and simulation results demonstrate the accuracy of theoretical analysis. They also show that the IRS-aided short-packet NOMA system outperforms the system without IRS, and that DPSs with 3-bit quantization achieve a similar performance as the optimal CPSs.

**Index Terms**—Non-orthogonal multiple access, intelligent reflecting surface, short-packet communications, Nakagami- $m$  fading.

## I. INTRODUCTION

Intelligent reflecting surface (IRS), which consists of a large number of passive reflective elements, has recently been recognized as one of the most promising techniques for the beyond fifth-generation (B5G) wireless networks, due to its capability to dynamically alter wireless channels and enhance the spectrum efficiency of wireless systems [1]. A prototype of the IRS-aided communication system consisting of 1100 controllable elements of the IRS was designed in [2], where the field trials verified the great potential of the IRS for the B5G wireless networks.

The performance of IRS-aided communications has been widely analyzed over the past few years. For example, [3] derived the symbol error probability and outage probability (OP) of the IRS-aided system with the instantaneous channel state information (CSI) over Rician fading. In [4], the authors analyzed the OP and ergodic capacity (EC) of the IRS-aided system over Nakagami- $m$  fading. Additionally, the impact of phase errors at the IRS on the symbol error probability was analyzed in [5]. Compared with the instantaneous CSI, the statistical CSI is much easier to be obtained in practice. Motivated by this, [6] analyzed the OP of an IRS-aided single-antenna system with the statistical CSI over Rician fading.

Apart from IRS, non-orthogonal multiple access (NOMA) has also been identified as a promising technology for the B5G wireless networks. Thus, it is natural to integrate IRS and NOMA into the design of emerging wireless systems. Against this background, [7] studied the impact of optimal continuous phase shifts (CPSs) and

random discrete phase shifts (DPSs) on the OP performance in an IRS-aided downlink two-user NOMA system. Moreover, [8] designed an energy-efficient scheme for an IRS-aided multiple-input single-output NOMA system. In addition, by utilizing the moment matching method to approximate the received signal-to-noise ratios (SNRs), the OP of an IRS-aided uplink two-user NOMA system over Nakagami- $m$  fading was derived in [9].

Short-packet communications (SPC) is a major feature of ultra-reliable and low-latency communications (URLLC), which is a vital scenario of the B5G wireless networks. Thus, it is worthwhile to explore the potential of using SPC, IRS and NOMA to accomplish URLLC. For SPC, the maximal achievable rate (MAR) depends on the blocklength and block error rate (BLER) [10]. It was further pointed out in [11] that the performance metrics used in the infinite blocklength regime, such as the OP and EC, cannot accurately predict the performance of SPC, and the optimal design of SPC systems relies on a refined analysis of the interplay among the BLER, MAR, and blocklength. Following [11], [12] and [13] studied the interplay among the average BLER, minimum blocklength, and optimal power allocation of short-packet NOMA systems in the single-antenna and multiple-antenna scenarios, respectively. Also, considering the advantage of IRS, [14] and [15] analyzed the MAR and average BLER of IRS-aided SPC systems over various fading. To the best knowledge of the authors, the performance of IRS-aided short-packet NOMA systems has not been investigated until very recently by [16], where the authors considered random and optimal CPSs.

We note that there are three limitations in [16]. First, [16] only considered Rayleigh fading, which is not a generalized fading model. Second, [16] did not optimize the blocklength and power allocation coefficients for the considered system. Third, [16] did not touch DPSs at the IRS, which is a more feasible option than CPSs for practical use. In order to overcome these limitations, we analyze the BLERs of an IRS-aided short-packet NOMA system over generalized Nakagami- $m$  fading, which encompasses Rayleigh fading as a special case. This analysis allows us to examine the impacts of both CPSs and DPSs on the average BLERs, optimal power allocation, and minimum common blocklength in the considered system. Using numerical and simulation results, we validate our theoretical analysis, demonstrate the superiority of the IRS-aided short-packet NOMA system over the system without IRS, and show the impact of quantization of DPSs on the achieved performance, especially compared to CPSs.

**Notations:**  $|x|$  and  $\arg(x)$  denote the modulus and angle of a complex number  $x$ , respectively.  $f_X(x)$ ,  $F_X(x)$  and  $\bar{X} = \mathbb{E}[X]$  denote the probability density function (PDF), cumulative distribution function (CDF) and expectation of a random variable (RV)  $X$ , respectively.  $Q(x) = \int_x^\infty \frac{1}{\sqrt{2\pi}} e^{-\frac{t^2}{2}} dt$  is the Gaussian  $Q$ -function.  $\Gamma(m)$  is the Gamma function.  $\mathcal{U}(a, b)$  denotes the uniform distribution over the interval  $(a, b)$ . Nakagami( $m, \Omega$ ) denotes the Nakagami- $m$  distribution with shape parameter  $m$  and average power  $\Omega$ . Gamma( $m, \Omega$ ) denotes the Gamma distribution, whose PDF is  $f_X(x) = \frac{\Omega^m x^{m-1} e^{-\Omega x}}{\Gamma(m)}$ .  $\mathcal{CN}(0, 1)$  and  $\mathcal{N}(0, 1)$  denote circularly-symmetric complex Gaussian and real Gaussian distributions with zero mean and unit variance, respectively.

This work was supported in part by the National Key R&D Program of China (2017YFE0118900). (*Corresponding author: Lei Yuan.*)

L. Yuan, Q. Du, and N. Yang are with the School of Information Science and Engineering, Lanzhou University, Lanzhou, 730000, Gansu, China. (e-mail: yuanl@lzu.edu.cn; duqy20@lzu.edu.cn; nyang20@lzu.edu.cn).

N. Yang is with the School of Engineering, Australian National University, Canberra, ACT 2600, Australia (e-mail: nan.yang@anu.edu.au).

F. Fang is with the Department of Electrical and Computer Engineering and the Department of Computer Science, Western University, London, ON N6A 3K7, Canada (e-mail: fang.fang@uwo.ca).

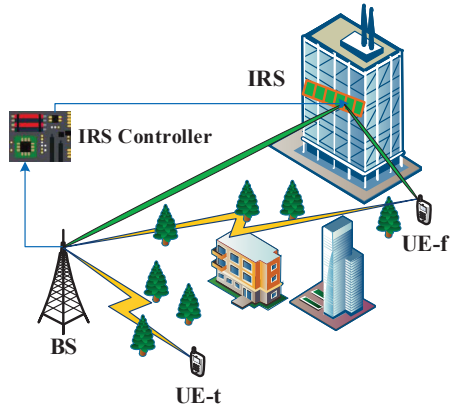


Fig. 1: The illustration of the considered IRS-aided downlink NOMA system.

## II. SYSTEM MODEL

This work considers an IRS-aided downlink NOMA system, as depicted in Fig. 1, where a single-antenna BS communicates with two single-antenna users. UE- $t$  and UE- $f$  represent the near user and the far user from the BS, respectively. Due to the long distance between the BS and UE- $f$ , a passive reflective IRS with  $N$  elements is used to improve the transmission quality between the BS and UE- $f$ .

We assume that all links undergo independent and identically distributed (i.i.d.) Nakagami- $m$  small-scale fading and have the same path-loss exponent  $\beta$ . The channel coefficient between the  $n$ th element of the IRS and the BS is denoted by  $g_{1n} \triangleq d_1^{-\beta/2} h_{1n}$  for all  $n \in \{1, \dots, N\}$ , where  $d_1$  denotes the distance between the BS and the center of the IRS and  $|h_{1n}| \sim \text{Nakagami}(m_1, 1)$ . Similarly, we denote the channel coefficient between the  $n$ th element of the IRS and UE- $f$  by  $g_{2n} \triangleq d_2^{-\beta/2} h_{2n}$ , where  $d_2$  denotes the distance between the center of the IRS and UE- $f$  and  $|h_{2n}| \sim \text{Nakagami}(m_2, 1)$ . The channel coefficient between the BS and UE- $k$ ,  $k \in \{t, f\}$ , is denoted by  $g_k \triangleq d_k^{-\beta/2} h_k$ , where  $d_k$  denotes the distance between the BS and UE- $k$  and  $|h_k| \sim \text{Nakagami}(m_k, 1)$ .

According to the principles of NOMA, the BS transmits  $s \triangleq (\sqrt{\alpha_t P_s} x_t + \sqrt{\alpha_f P_s} x_f)$  to two users, where  $P_s$  is the transmit power at the BS,  $x_k$  denotes the normalized signal sent to UE- $k$ ,  $\alpha_k$  denotes the power allocation coefficient for UE- $k$ , and  $\alpha_t + \alpha_f = 1$ . Thus, the received signals at UE- $t$  and UE- $f$  are expressed as

$$y_t = g_t s + w_t, \quad (1)$$

and

$$y_f = \left( \sum_{n=1}^N g_{1n} g_{2n} e^{j\Theta_n} + g_f \right) s + w_f = G_c s + w_f, \quad (2)$$

respectively, where  $G_c \triangleq \sum_{n=1}^N g_{1n} g_{2n} e^{j\Theta_n} + g_f$ ,  $\Theta_n \in [0, 2\pi)$  denotes the phase adjustment introduced by the  $n$ th element of the IRS, and  $w_k$  denotes the complex additive white Gaussian noise which follows  $\mathcal{CN}(0, \sigma^2)$ .

1) *Statistics of the end-to-end channel Between BS and UE- $f$ :* We assume that the instantaneous CSI is available at the system. Thus, coherent combination and the optimal CPSs at the IRS, given by  $\Theta_n = \arg(h_f) - \arg(h_{1n}) - \arg(h_{2n})$ , can be used to maximize the received SNR at UE- $f$ . which causes high implementation complexity in practice. To reduce such complexity, [5] suggested to use DPSs, although quantization errors are inevitable. With this use, the optimal DPSs at the IRS are given by  $\Theta_n = \arg(h_f) - \arg(h_{1n}) - \arg(h_{2n}) + \phi_n$ , where  $\phi_n$  denotes the quantization error which is modeled by uniform distribution. For  $q$  quantization bits,  $\phi_n \sim \mathcal{U}(-2^{-q}\pi, 2^{-q}\pi)$  [5].

In order to determine the distribution of the received SNR at UE- $f$ , we need to derive the distribution of  $|G_c|^2$ . To this end, we define  $H' \triangleq \sum_{n=1}^N e^{j\phi_n} |h_{1n}| |h_{2n}|$  and present the distribution of  $H'$  in the following lemma.

*Lemma 1:* When  $N$  is large and under the assumptions that  $\mathbb{E}[|h_{1n}|^2] = \mathbb{E}[|h_{2n}|^2] = 1$ ,  $a_1 \triangleq \mathbb{E}[|h_{1n}|] < 1$ ,  $a_2 \triangleq \mathbb{E}[|h_{2n}|] < 1$ ,  $h_{1n}$ ,  $h_{2n}$ , and  $\phi_n$  are mutually independent RVs, and  $\phi_n$  follows the same distribution  $\phi$  with zero-mean and  $p$ -order circular moments  $\varphi_p = \mathbb{E}[e^{jp\phi}]$ , we can approximate  $H' = U + jV$  as a non-circularly symmetric complex Gaussian RV, where  $U$  and  $V$  are independent RVs,  $U \sim \mathcal{N}(\mu, \sigma_U^2)$ ,  $V \sim \mathcal{N}(0, \sigma_V^2)$ ,  $\mu = N\varphi_1 a_1 a_2$ ,  $\sigma_U^2 = \frac{N}{2}(1 + \varphi_2 - 2\varphi_1^2 a_1^2 a_2^2)$ , and  $\sigma_V^2 = \frac{N}{2}(1 - \varphi_2)$ .

*Proof:* This lemma can be proved aided by [5, Appendix A]. ■

According to [5], if the IRS adopts the optimal CPSs, both  $\varphi_1$  and  $\varphi_2$  equal 1. In this case, substituting  $\varphi_1 = \varphi_2 = 1$  into *Lemma 1*,  $H'$  is actually approximated as a real Gaussian RV, i.e.,  $U \sim \mathcal{N}(Na_1 a_2, N(1 - a_1^2 a_2^2))$ , and  $V$  is zero. Differently, if the IRS adopts the optimal DPSs with  $q$  quantization bits,  $\varphi_1$  and  $\varphi_2$  equal  $\frac{\sin(2^{-q}\pi)}{2^{-q}\pi}$  and  $\frac{\sin(2^{-q+1}\pi)}{2^{-q+1}\pi}$ , respectively. After obtaining  $H'$ , we can use the moment matching method, which is shown in *Lemma 2*, to derive the distribution of  $|G_c|^2$ .

*Lemma 2:* When  $X$  is a non-negative RV with the first moment  $\mathbb{E}[X]$  and the second moment  $\mathbb{E}[X^2]$ , we can approximate  $X$  as Gamma( $m, \eta$ ), where the shape parameter is  $m = \frac{(\mathbb{E}[X])^2}{\mathbb{E}[X^2] - (\mathbb{E}[X])^2}$  and scale parameter is  $\eta = \frac{\mathbb{E}[X]}{\mathbb{E}[X^2] - (\mathbb{E}[X])^2}$ . Moreover, Gamma RVs satisfy the scaling property, i.e., the RV  $cY \sim \text{Gamma}(m, c\eta)$ .

*Proof:* This lemma can be proved with the aid of [9]. ■

Given  $|G_c|^2 = |(d_1 d_2)^{-\beta/2} (U + jV) + g_f|^2$ , by using both *Lemma 1* and *Lemma 2*, we can derive and present the distribution of  $|G_c|^2$  in the following theorem.

*Theorem 1:* For large  $N$ , the distribution of  $|G_c|^2$  is approximated as the Gamma distribution, which is characterized by two parameters  $m_c = \frac{(\mathbb{E}[|G_c|^2])^2}{\mathbb{E}[|G_c|^4] - (\mathbb{E}[|G_c|^2])^2}$  and  $\eta_c = \frac{\mathbb{E}[|G_c|^2]}{\mathbb{E}[|G_c|^4] - (\mathbb{E}[|G_c|^2])^2}$ , i.e.,  $|G_c|^2 \sim \text{Gamma}(m_c, \eta_c)$ .  $\mathbb{E}[|G_c|^2]$  and  $\mathbb{E}[|G_c|^4]$  are given by (A.1) and (A.2), respectively.

*Proof:* Please refer to Appendix A. ■

2) *Distributions of the received SINRs at UE- $t$  and UE- $f$ :* At each time slot, we define UE-1 as the user which possesses a larger end-to-end channel gain, and define  $\alpha_1$  as its power allocation coefficient. According to the rules of NOMA, the BS allocates a lower transmit power to UE-1, i.e.,  $\alpha_1 < 0.5$ . For example, if UE- $t$  possesses a larger channel gain, then UE- $t$  and  $\alpha_t$  are UE-1 and  $\alpha_1$ , respectively. We further define  $G_1$  and  $x_1$  as the end-to-end channel coefficient and signal for UE-1, respectively. Then, we have  $|G_1|^2 = \max(|G_c|^2, |g_t|^2)$ . Similarly, we define UE-2 as the user with a smaller end-to-end channel gain, and define  $\alpha_2$ ,  $G_2$ , and  $x_2$  as the power allocation coefficient, end-to-end channel coefficient, and signal for UE-2, respectively.

By using successive interference cancellation (SIC), UE-1 first recovers  $x_2$  by treating  $x_1$  as interference. The instantaneous signal-to-interference-plus-noise ratio (SINR) of decoding  $x_2$  at UE-1 is written as

$$\gamma_{1,2} = \frac{\alpha_2 |G_1|^2}{\alpha_1 |G_1|^2 + \rho^{-1}}, \quad (3)$$

where  $\rho = P_s/\sigma^2$  is the transmit SNR. If  $x_2$  is successfully decoded and removed, then the instantaneous SNR of decoding  $x_1$  at UE-1 is written as

$$\gamma_{1,1} = \alpha_1 \rho |G_1|^2. \quad (4)$$

At UE-2,  $x_2$  is decoded directly where  $x_1$  is treated as interference.

Then the received SINR of decoding  $x_2$  at UE-2 is given by

$$\gamma_{2,2} = \frac{\alpha_2 |G_2|^2}{\alpha_1 |G_2|^2 + \rho^{-1}}. \quad (5)$$

### III. PERFORMANCE ANALYSIS

In this section, we analyze the average BLERs in the considered IRS-aided short-packet NOMA system and accordingly evaluate the impacts of CPSs and DPSs on such BLERs, the optimal power allocation, and the minimum common blocklength. Given the blocklength  $L$ , the BLER  $\varepsilon$ , and the SNR  $\gamma$ , the MAR  $R(L, \gamma, \varepsilon)$  in bits per channel use (bpcu) is written as [10]

$$R(L, \gamma, \varepsilon) = C(\gamma) - \sqrt{\frac{V(\gamma)}{L}} Q^{-1}(\varepsilon) + O\left(\frac{\log_2 L}{L}\right), \quad (6)$$

where  $C(\gamma) = \log_2(1 + \gamma)$  denotes the Shannon capacity,  $V(\gamma) = (1 - (1 + \gamma)^{-2})(\log_2 e)^2$  is the channel dispersion,  $Q^{-1}(\cdot)$  is the inverse of the Gaussian  $Q$ -function, and  $O\left(\frac{\log_2 L}{L}\right)$  is the remaining terms of order  $\frac{\log_2 L}{L}$ , which can be omitted when  $L \geq 100$  [12].

In this work, we define  $T_i$  and  $L_i$  as the number of data bits and blocklength for UE- $i$ , respectively,  $i \in \{1, 2\}$ . Then, the MAR at UE- $i$  is expressed as  $R_i = T_i/L_i$ , and the instantaneous BLER corresponding to the link with the instantaneous SNR  $\gamma_{i,j}$ , denoted by  $\varepsilon_{i,j}$ ,  $j \in \{1, 2\}$ , is approximated as

$$\varepsilon_{i,j} \approx Q\left(\frac{C(\gamma_{i,j}) - R_j}{\sqrt{V(\gamma_{i,j})/L_j}}\right). \quad (7)$$

Furthermore, for wireless fading channels, the average BLER  $\bar{\varepsilon}_{i,j}$  can be written as

$$\bar{\varepsilon}_{i,j} \approx \int_0^\infty Q\left(\frac{C(x) - R_j}{\sqrt{V(x)/L_j}}\right) f_{\gamma_{i,j}}(x) dx, \quad (8)$$

where  $f_{\gamma_{i,j}}(x)$  denotes the PDF of  $\gamma_{i,j}$ .

It is noted that in URLLC the perfect SIC cannot be guaranteed and  $\bar{\varepsilon}_{i,j}$  is a very small value, e.g.,  $10^{-3}$  to  $10^{-5}$ , the average BLER of decoding  $x_1$  at UE-1 is approximated as

$$\bar{\varepsilon}_1 = \bar{\varepsilon}_{1,2} + (1 - \bar{\varepsilon}_{1,2}) \bar{\varepsilon}_{1,1} \approx \bar{\varepsilon}_{1,2} + \bar{\varepsilon}_{1,1}. \quad (9)$$

In order to find a closed-form expression for  $\bar{\varepsilon}_{i,j}$ , we approximate  $Q\left(\frac{C(\gamma_{i,j}) - R_j}{\sqrt{V(\gamma_{i,j})/L_j}}\right)$  as [12]

$$Z_{i,j}(\gamma_{i,j}) = \begin{cases} 1, & \gamma_{i,j} \leq v_j, \\ \frac{1}{2} - \kappa_j(\gamma_{i,j} - o_j), & v_j < \gamma_{i,j} < \mu_j, \\ 0, & \gamma_{i,j} \geq \mu_j, \end{cases} \quad (10)$$

where  $\kappa_j = \sqrt{L_j}/\sqrt{2\pi(2^{2R_j} - 1)}$ ,  $o_j = 2^{R_j} - 1$ ,  $v_j = o_j - \frac{1}{2\kappa_j}$ , and  $\mu_j = o_j + \frac{1}{2\kappa_j}$ . In this case, the average BLER  $\bar{\varepsilon}_{i,j}$  can be approximated as

$$\bar{\varepsilon}_{i,j} \approx \int_0^\infty Z_{i,j}(x) f_{\gamma_{i,j}}(x) dx \stackrel{(a)}{=} \kappa_j \int_{v_j}^{\mu_j} F_{\gamma_{i,j}}(x) dx \approx F_{\gamma_{i,j}}(o_j), \quad (11)$$

where  $F_{\gamma_{i,j}}(x)$  is the CDF of  $\gamma_{i,j}$ , step (a) is obtained by using the partial integration method, and step (b) is obtained by using the first-order Riemann integral approximation given by  $\int_a^b f(x) dx \approx (b - a)f\left(\frac{a+b}{2}\right)$  [12].

#### A. Average BLERs

By applying the order statistics, the expressions for  $F_{\gamma_{i,j}}$  are

$$F_{\gamma_{22}}(x) = 1 - \left(1 - \frac{\gamma\left(m_c, \frac{\eta_c x}{\rho(\alpha_2 - \alpha_1 x)}\right)}{\Gamma(m_c)}\right) \times \left(1 - \frac{\gamma\left(m_t, \frac{\eta_t x}{\rho(\alpha_2 - \alpha_1 x)}\right)}{\Gamma(m_t)}\right), \quad (12)$$

$$F_{\gamma_{12}}(x) = \frac{\gamma\left(m_c, \frac{\eta_c x}{\rho(\alpha_2 - \alpha_1 x)}\right) \gamma\left(m_t, \frac{\eta_t x}{\rho(\alpha_2 - \alpha_1 x)}\right)}{\Gamma(m_c) \Gamma(m_t)}, \quad (13)$$

and

$$F_{\gamma_{11}}(x) = \frac{\gamma\left(m_c, \frac{\eta_c x}{\alpha_1 \rho}\right) \gamma\left(m_t, \frac{\eta_t x}{\alpha_1 \rho}\right)}{\Gamma(m_c) \Gamma(m_t)}, \quad (14)$$

where  $\eta_t = m_t/d_t^\beta$  and the power allocation coefficients need to satisfy the condition  $\alpha_2 - \alpha_1 x > 0$ . By using such expressions, the approximate average BLER of decoding  $x_2$  at UE-2, denoted by  $\bar{\varepsilon}_2$ , is derived as

$$\bar{\varepsilon}_2 = \bar{\varepsilon}_{2,2} \approx 1 - \left(1 - \frac{\gamma(m_c, \eta_c \varrho_2)}{\Gamma(m_c)}\right) \left(1 - \frac{\gamma(m_t, \eta_t \varrho_2)}{\Gamma(m_t)}\right), \quad (15)$$

where  $\varrho_2 = \frac{o_2}{\rho(\alpha_2 - \alpha_1 o_2)}$ . Moreover, the approximate average BLER of decoding  $x_1$  at UE-1, denoted by  $\bar{\varepsilon}_1$ , is derived as

$$\begin{aligned} \bar{\varepsilon}_1 &\approx \bar{\varepsilon}_{1,1} + \bar{\varepsilon}_{1,2} \\ &\approx \frac{\gamma(m_c, \eta_c \varrho_1) \gamma(m_t, \eta_t \varrho_1) + \gamma(m_c, \eta_c \varrho_2) \gamma(m_t, \eta_t \varrho_2)}{\Gamma(m_c) \Gamma(m_t)}, \end{aligned} \quad (16)$$

where  $\varrho_1 = \frac{o_1}{\rho \alpha_1}$ .

In the high SNR regime, by using  $\frac{\gamma(s,x)}{x^s} \rightarrow \frac{1}{s}$  for  $x \rightarrow 0$  [17] and (11), the asymptotic expressions for the average BLER at both users are derived. Specifically, the asymptotic average BLER of decoding  $x_2$  at UE-2, denoted by  $\bar{\varepsilon}_2^\infty$ , is derived as

$$\bar{\varepsilon}_2^\infty \approx \begin{cases} \frac{(\eta_c \varrho_2)^{m_c}}{\Gamma(m_c + 1)}, & m_t > m_c, \\ \frac{(\eta_t \varrho_2)^{m_t}}{\Gamma(m_t + 1)}, & m_t < m_c, \\ \frac{\varrho_2^{m_t}}{\Gamma(m_t + 1)} (\eta_t^{m_t} + \eta_c^{m_t}), & m_t = m_c. \end{cases} \quad (17)$$

Moreover, the asymptotic average BLER of decoding  $x_1$  at UE-1, denoted by  $\bar{\varepsilon}_1^\infty$ , is derived as

$$\bar{\varepsilon}_1^\infty \approx \frac{\eta_t^{m_t} \eta_c^{m_c} (\varrho_1^{m_t + m_c} + \varrho_2^{m_t + m_c})}{\Gamma(m_t + 1) \Gamma(m_c + 1)}. \quad (18)$$

Based on (17) and (18), the diversity order at UE-2 and UE-1 are obtained as

$$-\lim_{\rho \rightarrow \infty} \frac{\log \bar{\varepsilon}_2^\infty}{\log \rho} = \begin{cases} m_t, & m_t \leq m_c, \\ m_c, & m_t > m_c, \end{cases} \quad (19)$$

and

$$-\lim_{\rho \rightarrow \infty} \frac{\log \bar{\varepsilon}_1^\infty}{\log \rho} = m_t + m_c, \quad (20)$$

respectively.

#### B. Power Allocation and Blocklength Optimization at High SNRs

We denote  $\bar{\varepsilon}_i^{th}$  as the average BLER threshold at UE- $i$ , and apply them into (17) and (18) to obtain the minimum blocklength  $L_{i,\min}$  of UE- $i$  at high SNRs as

$$L_{2,\min} \approx \frac{T_2}{\log_2\left(\frac{1+\xi}{1+\alpha_1 \xi}\right)} \quad (21)$$

and

$$L_{1,\min} \approx \frac{T_1}{\log_2\left(\alpha_1 \rho \left(\psi \bar{\varepsilon}_1^{th} - \left(\frac{\xi}{\rho}\right)^{m_t + m_c}\right)^{\frac{1}{m_t + m_c}} + 1\right)}, \quad (22)$$

where  $\psi = \frac{\Gamma(m_t + 1) \Gamma(m_c + 1)}{\eta_t^{m_t} \eta_c^{m_c}}$  and

$$\xi = \begin{cases} \frac{\rho}{\eta_t} (\bar{\varepsilon}_2^{th} \Gamma(m_t + 1))^{\frac{1}{m_t}}, & m_t < m_c, \quad (23a) \\ \frac{\rho}{\eta_c} (\bar{\varepsilon}_2^{th} \Gamma(m_c + 1))^{\frac{1}{m_c}}, & m_t > m_c, \quad (23b) \\ \rho (\bar{\varepsilon}_2^{th} \Gamma(m_t + 1) / (\eta_t^{m_t} + \eta_c^{m_c}))^{\frac{1}{m_t}}, & m_t = m_c. \quad (23c) \end{cases}$$

**Algorithm 1:** Power Allocation Algorithm

---

**Input:** input parameters  $N, T_1, T_2, m_t, m_f, m_1, m_2, d_t, d_f, d_1, d_2, \beta, q, \rho, \bar{\varepsilon}_1^{th}, \bar{\varepsilon}_2^{th}$ , and tolerance  $\mu$ .

**Output:** Optimal power allocation coefficient  $\alpha_1^*$ .

- 1 Initialize:  $\alpha^- \leftarrow 0, \alpha^+ \leftarrow 0.5$ , and  $\hat{\alpha} \leftarrow \frac{\alpha^- + \alpha^+}{2}$ ;
- 2 **while**  $|L_{2,\min} - L_{1,\min}| > \mu$  **do**
- 3   **if**  $L_{2,\min} - L_{1,\min} < 0$  **then**
- 4     Set  $\alpha^- \leftarrow \hat{\alpha}$ ;
- 5   **else**
- 6     Set  $\alpha^+ \leftarrow \hat{\alpha}$ ;
- 7   **end**
- 8   Set  $\hat{\alpha} \leftarrow \frac{\alpha^- + \alpha^+}{2}$  and compute  $L_{2,\min} - L_{1,\min}$  based on (21) and (22);
- 9 **end**
- 10 Set  $\alpha_1^* \leftarrow \hat{\alpha}$ ;
- 11 **return**  $\alpha_1^*$ .

---

By calculating the derivative of  $L_{2,\min}$  with respect to  $\alpha_1$ , we obtain

$$\frac{\partial L_{2,\min}}{\partial \alpha_1} \approx \frac{T_2 \xi}{(1 + \alpha_1 \xi) \left( \log_2 \left( \frac{1 + \xi}{1 + \alpha_1 \xi} \right) \right)^2 \ln 2} > 0, \quad (24)$$

which shows that  $L_{2,\min}$  is an increasing function of  $\alpha_1$ . Then by calculating the derivative of  $L_{1,\min}$  with respect to  $\alpha_1$ , we obtain

$$\frac{\partial L_{1,\min}}{\partial \alpha_1} \approx - \frac{T_1 \vartheta}{(\alpha_1 \vartheta + 1) (\log_2 (\alpha_1 \vartheta + 1))^2 \ln 2} < 0 \quad (25)$$

with

$$\vartheta = \rho \left( \psi \bar{\varepsilon}_1^{th} \right)^{\frac{1}{m_t + m_c}}, \quad (26)$$

which shows that  $L_{1,\min}$  is a decreasing function of  $\alpha_1$ . Therefore, the minimum common blocklength  $L^*$  is obtained by solving  $L^* = L_{1,\min} = L_{2,\min}$ .

Based on [13], the optimal power allocation coefficient  $\alpha_1^*$ , corresponding to  $L^*$ , can be obtained by using the bisection search shown in **Algorithm 1**. After doing so, we substitute  $\alpha_1^*$  into (21),  $L^*$  can be expressed as

$$L^* \approx \frac{T_2}{\log_2 \left( \frac{1 + \xi}{1 + \alpha_1^* \xi} \right)} \quad (27)$$

#### IV. NUMERICAL RESULTS

In this section, we provide numerical and simulation results to validate our analysis in Section III, and offer some useful insights into system design. The simulation parameters are set as follows:  $\beta = 4, m_1 = m_2 = 4, m_f = 1, d_1 = 25, d_2 = 10, d_f = 30, T_1 = T_2 = 200, L_1 = L_2 = 300$ , and  $\mu = 10^{-3}$ . Other parameters are specified in each figure.

To show the accuracy of our derived expressions for the average BLER, Fig. 2 plots the average BLER versus  $\rho$  for the considered IRS-aided short-packet NOMA system with the optimal CPSs, where  $\alpha_1 = 0.2, m_t = 3.5, d_t = 15$  and  $N = 32$  or  $96$ . We first observe that, the analytical curves derived from (15) and (16) match perfectly with simulation results over the entire transmit SNR range, and the asymptotic curves derived from (17) and (18) accurately predict the average BLERs in the high transmit SNR regime. These observations demonstrate the correctness of our analysis. Second, we observe from this figure that, compared to the system without IRS, the IRS-aided system achieves lower BLERs for both users at the same transmit SNR. Third, we observe that when the number of elements of the IRS increases, the performance improvement becomes more profound, at the cost of increasing implementation complexity.

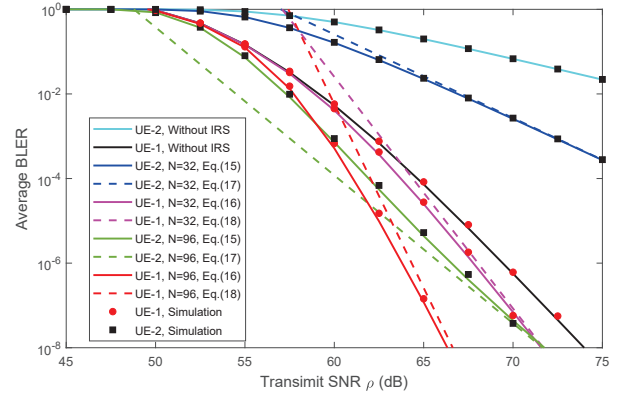


Fig. 2: Average BLER versus  $\rho$  for  $N = 32, N = 96$ , and the system without the use of IRS.

In Fig. 3, we study the impact of DPSs on the average BLER. In this figure, we use  $\alpha_1 = 0.2, m_t = 4$ , and  $d_t = 10$ . Specifically, Fig. 3(a) plots the average BLER versus  $\rho$  for the optimal CPSs, the DPSs with  $q = 1$  or  $q = 3$ , and  $N = 64$ . We observe from this subfigure that, on the one hand, the analytical curves corresponding to the DPSs are consistent with simulation results, which verifies our theoretical analysis. On the other hand, the BLER performance of DPSs with 3-bit quantization approaches to that of the optimal CPSs, implying that using the 3-bit quantizer is sufficient to achieve the near-optimal performance in practice. Furthermore, we examine the impact of the number of quantization bits on the required number of elements of IRS for achieving a target BLER. Since the impact on two users is similar, we only plot the average BLER versus the number of elements of the IRS for UE-2 in Fig. 3(b). As shown in this subfigure, to achieve the BLER of  $10^{-5}$  at UE-2, the required numbers of elements of the IRS for DPSs with 1-bit, 2-bit, and 3-bit quantizers are 169, 119, and 110, respectively. This observation demonstrates that, compared to using the 1-bit quantizer, using the 3-bit quantizer can save 59 elements of the IRS for achieving  $\bar{\varepsilon}_2 = 10^{-5}$ , while the tradeoff between the required number of quantization bits and the required number of elements of the IRS depends on practical implementation complexity.

Fig. 4 shows the impact of DPSs on  $L_{i,\min}$  for different  $\alpha_1$  in the high transmit SNR regime. The parameters are  $m_t = 3.5, d_t = 15, \bar{\varepsilon}_1^{th} = \bar{\varepsilon}_2^{th} = 10^{-5}$ , and  $q = 1, 2, 3$ . In Fig. 4(a), we assume  $N = 128$  and  $\rho = 67$  dB. Using *Theorem 1*, we obtain  $m_c = 4.3, 6.5$ , and  $7.2$  for  $q = 1, 2$ , and  $3$ , respectively. Since  $m_t < m_c$ , according to (21) and (23a), the curve corresponding to  $L_{2,\min}$  is unchanged for different values of  $q$ . Moreover, we observe from this subfigure that  $L^*$  decreases from 176 to 158 when  $q$  increases from 1 to 3. In Fig. 4(b), we assume  $N = 64$  and  $\rho = 72$  dB. Similarly, we obtain  $m_c = 2.3, 3.1$ , and  $3.3$  for  $q = 1, 2$ , and  $3$ , respectively. Since  $m_t > m_c$ , according to (21), (22), and (23b), we find that the value of  $q$  affects both  $L_{2,\min}$  and  $L_{1,\min}$ . Furthermore, we observe from this subfigure that  $L^*$  decreases from 740 to 203 when  $q$  increases from 1 to 3. These observations show that quantization errors impose a profound impact on achieving low-latency transmission for the case of  $m_t > m_c$ .

#### V. CONCLUSION

This paper analyzed the performance of IRS-aided short-packet NOMA systems over Nakagami- $m$  fading channels. We first analyzed the statistical property of the end-to-end channel in the considered IRS-aided system, based on which we derived the approximate closed-form expressions for the average BLER at both users, as

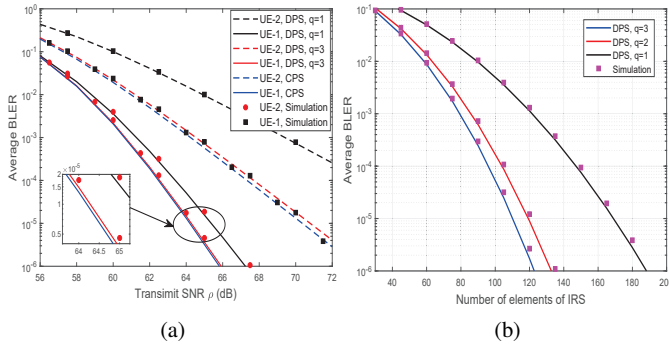


Fig. 3: Impact of DPSs on the average BLER. (a) Average BLER versus  $\rho$  for  $N = 64$ . (b) Average BLER at UE-2 versus  $N$  for  $q = 1, 2, 3$ .

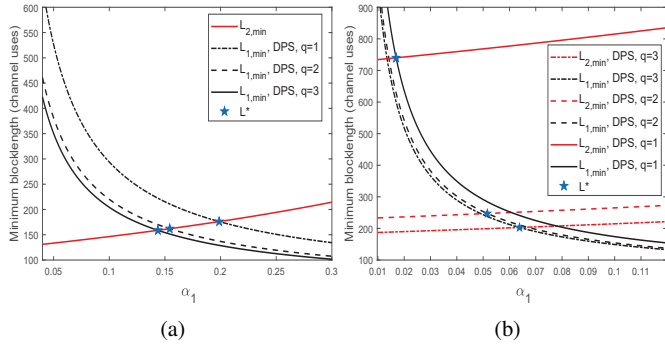


Fig. 4: Minimum blocklength versus  $\alpha_1$  for (a)  $m_t < m_c$  and (b)  $m_t > m_c$ .

well as the asymptotic expressions for the average BLER at high transmit SNRs. Using the asymptotic expressions, we quantified the relationship among the minimum common blocklength, optimal power allocation, and the parameters of the IRS for achieving the target BLERs at two users. Finally, numerical and simulation results validated our theoretical analysis, and demonstrated that (i) IRS-aided short-packet NOMA systems outperform the systems without IRS in terms of reliability and (ii) DPSs with 3-bit quantization are sufficient to achieve the near-optimal performance. Considering that the statistical CSI is much easily obtained at the BS and reduces feedback latency, the design of IRS-aided short-packet NOMA systems with statistical CSI will be investigated in the future work.

#### APPENDIX A PROOF OF THEOREM 1

Let us define  $U_1 = (d_1 d_2)^{-\beta/2} U$  and  $V_1 = (d_1 d_2)^{-\beta/2} V$ , and then rewrite  $|G_c|^2$  as  $|G_c|^2 = (U_1 + |g_f|)^2 + V_1^2$ . Using the scaling property, we find that  $|g_f| \sim \text{Nakagami}(m_f, d_f^{-\beta})$ ,  $U_1 \sim \mathcal{N}((d_1 d_2)^{-\beta/2} \mu, (d_1 d_2)^{-\beta} \sigma_U^2)$ , and  $V_1 \sim \mathcal{N}(0, (d_1 d_2)^{-\beta} \sigma_V^2)$ . Thus, we obtain the expectation of  $|G_c|^2$  and  $|G_c|^4$  as

$$\mathbb{E}[|G_c|^2] = \mathbb{E}[|g_f|^2] + \mathbb{E}[U_1^2] + 2\mathbb{E}[|g_f|] \mathbb{E}[U_1] + \mathbb{E}[V_1^2] \quad (\text{A.1})$$

and

$$\begin{aligned} \mathbb{E}[|G_c|^4] &= \mathbb{E}[|g_f|^4] + \mathbb{E}[U_1^4] + 6\mathbb{E}[|g_f|^2] \mathbb{E}[U_1^2] \\ &\quad + 4\mathbb{E}[|g_f|^3] \mathbb{E}[U_1] + 4\mathbb{E}[|g_f|] \mathbb{E}[U_1^3] \\ &\quad + 2\mathbb{E}[V_1^2] \mathbb{E}[|g_f|^2] + 2\mathbb{E}[V_1^2] \mathbb{E}[U_1^2] \\ &\quad + 4\mathbb{E}[V_1^2] \mathbb{E}[|g_f|] \mathbb{E}[U_1] + \mathbb{E}[V_1^4], \end{aligned} \quad (\text{A.2})$$

respectively. According to [18], if a real Gaussian RV  $Z_1$  follows  $\mathcal{N}(0, \sigma_{Z_1}^2)$ , then the  $p$ th moment of  $Z_1$  is

$$\mathbb{E}[Z_1^p] = \begin{cases} \frac{p!}{(p/2)!} \left(\frac{\sigma_{Z_1}}{\sqrt{2}}\right)^p, & \text{when } p \text{ is even,} \\ 0, & \text{when } p \text{ is odd.} \end{cases} \quad (\text{A.3})$$

Furthermore, if  $Z_2 = b + Z_1$ , where  $b$  is a non-zero constant number (i.e.,  $Z_2 \sim \mathcal{N}(b, \sigma_{Z_1}^2)$ ), then the  $p$ th moment of  $Z_2$  is

$$\mathbb{E}[Z_2^p] = \mathbb{E}[(b + Z_1)^p] = \sum_{k=0}^p C_p^k b^k \mathbb{E}[Z_1^{p-k}]. \quad (\text{A.4})$$

According to [9], if  $Z_3 \sim \text{Nakagami}(m_z, \Omega_z)$ , then the  $p$ th moment of  $Z_3$  is

$$\mathbb{E}[Z_3^p] = \frac{\Gamma(m_z + \frac{p}{2})}{\Gamma(m_z) (m_z/\Omega_z)^{p/2}}. \quad (\text{A.5})$$

By using  $\varphi_i = 1$  for the optimal CPSs,  $\varphi_i = \frac{\sin(2-q+i-1\pi)}{2-q+i-1\pi}$  for the optimal DPSs, and Lemma 1, we obtain the parameters of  $U_1$  and  $V_1$  in different cases. Then, by substituting (A.3), (A.4), and (A.5) into (A.1) and (A.2), we derive  $\mathbb{E}[|G_c|^2]$  and  $\mathbb{E}[|G_c|^4]$ , respectively.

#### REFERENCES

- [1] Q. Wu, S. Zhang, B. Zheng, C. You and R. Zhang, "Intelligent reflecting surface-aided wireless communications: a tutorial," *IEEE Trans. Commun.*, vol. 69, no. 5, pp. 3313-3351, May 2021.
- [2] X. Pei et al., "RIS-aided wireless communications: prototyping, adaptive beamforming, and indoor/outdoor field trials," *IEEE Trans. Commun.*, vol. 69, no. 12, pp. 8627-8640, Dec. 2021.
- [3] A. M. Salhab and M. H. Samuh, "Accurate performance analysis of reconfigurable intelligent surfaces over Rician fading channels," *IEEE Wireless Commun. Lett.*, vol. 10, no. 5, pp. 1051-1055, May 2021.
- [4] D. Selimis, K. P. Peppas, G. C. Alexandropoulos and F. I. Lazarakis, "On the performance analysis of RIS-empowered communications over Nakagami- $m$  fading," *IEEE Commun. Lett.*, vol. 25, no. 7, pp. 2191-2195, July 2021.
- [5] M.A. Badiu and J. P. Coon, "Communication through a large reflecting surface with phase errors," *IEEE Wireless Commun. Lett.*, vol. 9, no. 2, pp. 184-188, Feb. 2020.
- [6] P. Xu, W. Niu, G. Chen, Y. Li and Y. Li, "Performance analysis of RIS-assisted systems with statistical channel state information," *IEEE Trans. Veh. Technol.*, vol. 71, no. 1, pp. 1089-1094, Jan. 2022.
- [7] Z. Ding, R. Schober and H. V. Poor, "On the impact of phase shifting designs on IRS-NOMA," *IEEE Wireless Commun. Lett.*, vol. 9, no. 10, pp. 1596-1600, Oct. 2020.
- [8] F. Fang, Y. Xu, Q. -V. Pham and Z. Ding, "Energy-Efficient Design of IRS-NOMA Networks," *IEEE Trans. Veh. Technol.*, vol. 69, no. 11, pp. 14088-14092, Nov. 2020.
- [9] B. Tahir, S. Schwarz and M. Rupp, "Analysis of uplink IRS-assisted NOMA under Nakagami- $m$  fading via moments matching," *IEEE Wireless Commun. Lett.*, vol. 10, no. 3, pp. 624-628, Mar. 2021.
- [10] Y. Polyanskiy, H. V. Poor and S. Verdú, "Channel coding rate in the finite blocklength regime," *IEEE Trans. Info. Theory*, vol. 56, no. 5, pp. 2307-2359, May 2010.
- [11] G. Durisi, T. Koch, J. Ostman, Y. Polyanskiy and W. Yang, "Short-packet communications over multiple-antenna Rayleigh-fading channels," *IEEE Trans. Commun.*, vol. 64, no. 2, pp. 618-629, Feb. 2016.
- [12] Y. Yu, H. Chen, Y. Li, Z. Ding, and B. Vucetic, "On the performance of non-orthogonal multiple access in short-packet communications," *IEEE Commun. Lett.*, vol. 22, no. 3, pp. 590-593, Mar. 2018.
- [13] D. D. Tran, S. K. Sharma, S. Chatzinotas, "Short-packet communications for MIMO NOMA systems over Nakagami- $m$  fading: BLER and minimum blocklength analysis," *IEEE Trans. Veh. Technol.*, vol. 70, no. 4, pp. 3583-3598, Apr. 2021.
- [14] R. Hashemi, S. Ali, N. H. Mahmood and M. Latva-aho, "Average rate and error probability analysis in short packet communications over RIS-aided URLLC systems," *IEEE Trans. Veh. Technol.*, vol. 70, no. 10, pp. 10320-10334, Oct. 2021.
- [15] H. Ren, K. Wang and C. Pan, "Intelligent reflecting surface-aided URLLC in a factory automation scenario," *IEEE Trans. Commun.*, vol. 70, no. 1, pp. 707-723, Jan. 2022.
- [16] T. -H. Vu, T. -V. Nguyen, D. B. Da Costa and S. Kim, "Intelligent reflecting surface-aided short-packet non-orthogonal multiple access systems," *IEEE Trans. Veh. Technol.*, doi: 10.1109/TVT.2022.3146856.
- [17] I. Gradshteyn and I. Ryzhik, *Table of Integrals, Series, and Products*, 7th ed. Academic Press, Mar. 2007.
- [18] H. Stark and J. Woods, *Probability and Random Processes with Applications to Signal Processing and Communications*, Jul. 2001.